Fusion hindrance for ^{27}Al + ^{45}Sc and other systems with a positive Q value

C. L. Jiang,[1] K. E. Rehm,[1] H. Esbensen,[1] B. B. Back,[1] R. V. F. Janssens,[1] P. Collon,[2] C. M. Deibel,[1,3] B. DiGiovine,[1] J. M. Figueira,[1,4] J. P. Greene,[1] D. J. Henderson,[1] H. Y. Lee,[1,*] M. Notani,[2] S. T. Marley,[1,5] R. C. Pardo,[1] N. Patel,[1,6] D. Seweryniak,[1] X. D. Tang,[2] C. Ugalde,[1] and S. Zhu[1]

[1]*Physics Division, Argonne National Laboratory, Argonne, Illinois 60439, USA*

[2]*University of Notre Dame, Notre Dame, Indiana 46556, USA*

[3]*Joint Institute for Nuclear Astrophysics, Michigan State University, East Lansing, Michigan 48824, USA*

[4]*TANDAR, Buenos Aires, Argentina*

[5]*Western Michigan University, Kalamazoo, Michigan 49008, USA*

[6]*Department of Physics, Colorado School of Mines, Golden, Colorado 80401, USA*

(Received 7 December 2009; published 24 February 2010)

Fusion evaporation cross sections for the ^{27}Al + ^{45}Sc (Q = 9.63 MeV) system are measured down to about 300 nb. Deviations from standard coupled-channels calculations were observed in this system at the lowest energies. The steep fall-off of the fusion cross sections can be reproduced by calculations using a shallow potential model, which was originally developed to explain the hindrance behavior of heavy-ion fusion in medium-mass systems with negative Q values. Comparisons of the hindrance behavior between the present experiment and other systems, for example, ^{28}Si + ^{30}Si (Q = 14.3 MeV) and ^{36}S + ^{48}Ca (Q = 7.55 MeV) are presented.

DOI: 10.1103/PhysRevC.81.024611 PACS number(s): 25.70.Jj, 26.20.Np, 24.10.Eq, 24.10.Ht

I. INTRODUCTION

Hindrance in heavy-ion fusion at extreme subbarrier energies has become a subject of interest in nuclear reaction studies in recent years. This phenomenon, characterized by an S-factor maximum [$S(E) = \sigma E \exp(2\pi\eta)$] was first observed in medium-mass systems [1]. However, later measurements and analyses [2–8] showed that this represents a general behavior of heavy-ion fusion at extreme subbarrier energies. The systematics developed for a wide mass region showed that fusion hindrance is closely related to the entrance channel properties [5,6,8]. It can also affect fusion reaction rates that are of importance in nuclear astrophysics such as fusion between ^{12}C and ^{16}O [7,9] and reactions occurring in the crust of accreting neutron stars [10].

There is, however, an important difference between the medium-mass systems studied earlier and the astrophysically important fusion reactions coming from the fusion Q values: These are positive for lighter systems and negative for the heavier ones studied previously. From the asymptotic behavior of the S factor it is known that there must be an S-factor maximum for all systems with negative fusion Q value. While close to the barrier, the S factor always increases rapidly with decreasing energy, at $E = -Q$ the S factor must be zero. Thus, for these negative-Q-value systems, energy conservation blocks the fusion process at $E < -Q$. For a positive-Q-value system, however, there is no restriction on $S(E)$ for $E \to 0$ and therefore it is not necessary to have an S-factor maximum at low energies. Fusion in astrophysical environments usually occurs at temperatures that correspond to energies that are lower than what was studied in the laboratory. Consequently, one has to extrapolate the experimental results to lower energies to obtain the astrophysical reaction rates. The detailed behavior for these systems at low energies is very important since it will guide the extrapolation procedure.

In an earlier experiment, the fusion excitation function of the system ^{28}Si + ^{30}Si (Q = 14.3 MeV) was measured only down to ∼50 μb [11] because the background from reactions on the ^{12}C and ^{16}O contaminants prevented an extension of the measurements to lower energies. An indication of fusion hindrance was observed since the cross sections drop much faster than predicted by standard coupled-channels (CC) calculations. However, no evidence of an S-factor maximum is found in this experiment.

Measurements for the system ^{36}S + ^{48}Ca (Q = 7.55 MeV) were reported by Stefanini *et al.* [12]. The cross section was measured down to about 600 nb. The behavior for this system at low energies is different from what was seen in the medium-mass nuclei; the logarithmic derivative $L(E)$ saturates and does not reach the value expected for a constant S factor (i.e., no S-factor maximum was found in the measured energy region). In the neighboring system ^{48}Ca + ^{48}Ca [13], which has a negative Q value for fusion, the measured $L(E)$ is very similar to the one for ^{36}S + ^{48}Ca. No S-factor maximum is observed either in the cross section range above ∼300 nb.

To investigate fusion hindrance for other systems with positive Q values, we measured the system ^{27}Al + ^{45}Sc (Q = 9.63 MeV). Since this system is closer in mass to ^{28}Si + ^{64}Ni, which was measured down to 26 nb, we expected to reach lower cross sections than achieved for ^{28}Si + ^{30}Si. Furthermore, Sc is a mono-isotopic element, which is helpful in these low cross-section measurements (see discussions in Ref. [1]).

The experimental procedure and the results are described in Sec. II. Comparisons with theoretical calculations are provided in Sec. III. Measurements of other fusion systems with positive Q values are discussed in Sec. IV. Finally, a short conclusion is presented in Sec. V.

*Present address: Los Alamos National Lab, Los Alamos, NM 87545, USA.

II. EXPERIMENTAL PROCEDURE AND RESULTS

The experiment was performed at the superconducting linear accelerator ATLAS at Argonne National Laboratory. The experimental setup and procedures were similar to those used in earlier measurements of the fusion-evaporation excitation functions for the systems ^{28}Si + ^{30}Si ($Q = 14.3$ MeV) [11], ^{28}Si + ^{64}Ni ($Q = -1.78$ MeV), and ^{64}Ni + ^{100}Mo ($Q = -92.3$ MeV) [1]. The evaporation residues were measured with the Fragment Mass Analyzer (FMA) [14] placed at 0° with respect to the beam direction. This spectrometer has a split-anode in the first electric dipole to suppress background events originating from beam particles scattered off the first anode. The ^{27}Al beams were in the energy range of 51–82 MeV. Thin, mono-isotopic ^{45}Sc targets, with thicknesses of 31 or 61 μg/cm^2 (evaporated on 20 μg/cm^2 carbon foils) were used. This minimized target thickness corrections in the energy regime where a steep fall-off in the excitation function occurs. A 40 μg/cm^2 carbon foil, 10 cm downstream from the target, served as a reset foil. Two surface-barrier Si detectors located at ±45° with respect to the beam direction were used for cross-section normalization.

The evaporation residues were detected and identified behind the FMA with detectors of the configuration PGAC$_1$-TIC$_1$-PGAC$_2$-TIC$_2$-PGAC$_3$-IC (see Ref. [15] for further details). Here, PGAC stands for an x-y position-sensitive, parallel-grid avalanche counter, TIC for a transmission ionization chamber, and IC for a large volume multi-anode ionization chamber. The first PGAC$_1$ counter was mounted at the focal-plane of the FMA where the evaporation residues are dispersed according to their mass-to-charge ratio M/q.

Full charge-state distributions were measured for four energies, while three to five charge states were recorded for six intermediate points. At the six lowest energies, only one or two charge states were measured. These data proved sufficient to determine the charge-state fractions of the detected evaporation residues with the required accuracy. The fusion residues measured in the focal plane detectors were identified using time-of-flight signals, ΔE signals, and the X-position signal at the focal plane, which was used to determine the M/q value of the detected particles.

To determine the FMA transmission it is necessary to characterize the angular distribution of the evaporation residues. In the present experiment this was achieved by using the statistical model code PACE [16]. It was found that the total angular distribution changes very little over the range of beam energies measured thus making the efficiency corrections simpler.

The background appearing in the measurements originated mostly from the carbon and oxygen contaminants in the target. At low energies, the particle identification of the evaporation residues in the focal plane detector of the FMA becomes challenging, especially for lighter target nuclei where the mass difference between the reaction products from the target and from carbon or oxygen contaminants is small. For the system ^{28}Si + ^{64}Ni, the cross section was measured down to about 26 nb [1], while a level of only 42 μb was reached for the lighter system ^{28}Si + ^{30}Si. The lowest cross section measured in the present experiment was 307 nb (i.e., between the two other systems).

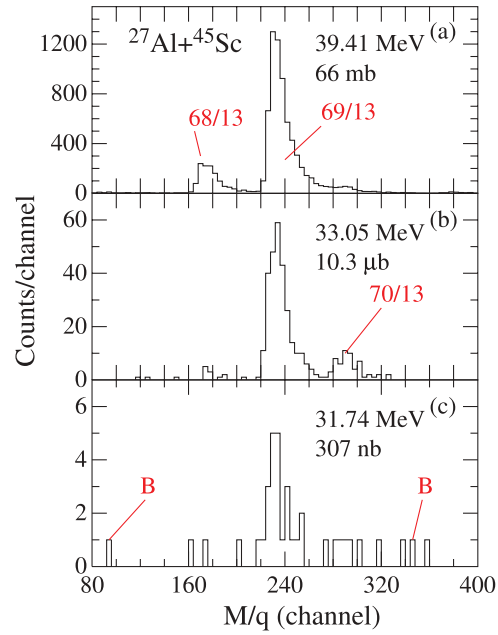

FIG. 1. (Color online) M/q spectra at the focal plane of the Fragment Mass Analyzer for three incident beam energies. Here M and q are the mass number and charge state of the evaporation residues measured at the focal-plane detector. The counts at the lowest energy $E = 31.74$ MeV, marked B, are background events.

Three M/q spectra at different incident beam energies are given in Fig. 1. These spectra are all obtained using gates on signals of various ΔE and time-of-flight measurements in the Parallel Plate Avalanche Counter (PPAC)-Ionization Chamber Stack at the FMA focal plane. The cross sections at these energies are 66 mb, 10.3 μb, and 307 nb, respectively. The positions for residues with $M/q = 68/13$, $69/13$, and $70/13$ are marked in Fig. 1(a) and 1(b). While the upper two spectra are practically free of background, the spectrum at the lowest energy [Fig. 1(c)] is contaminated by background events. There are counts at the values $M/q = 71/13$ and $< 67/13$, where no events are expected. Another indication of the background contribution comes from the relative yields of the mass peaks at $M/q = 68/13$ and $70/13$ (relative to the yields at $M/q = 69/13$), which should change smoothly and monotonically with energy. Experimentally, one finds that the ratios at this energy are abnormally large. It is estimated that, at this energy, the background contributions are about 28% resulting in an uncertainty in the cross section of 40%. For measurements at even lower energies, the "good" events decrease rapidly and the background dominates preventing the extension of the excitation function further toward lower energies.

The experimental cross sections as a function of center-of-mass energy E are presented in Fig. 2. While the normalization of the data in the most interesting energy region, below 66 MeV, is straightforward, one has to consider that, for the four data points at higher energies, the elastic scattering at the monitor angles of 45° is not pure Rutherford. In this energy range, elastic scattering cross sections at $\theta_{\rm lab} = 45°$ from optical model calculations with a set of universal potential

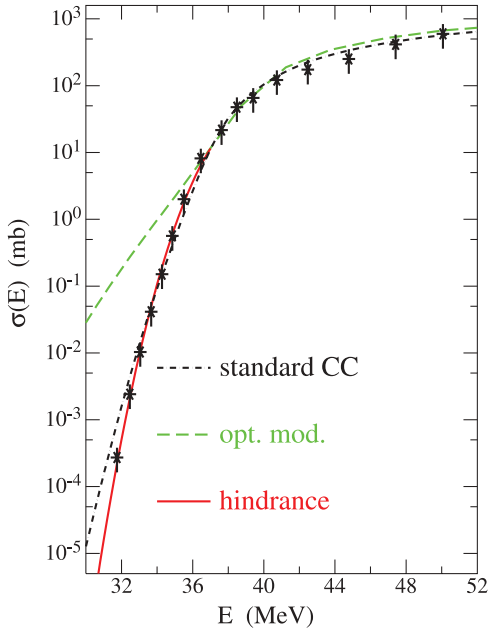

FIG. 2. (Color online) Comparisons of experimental evaporation residue cross sections with calculations for the system ^{27}Al + ^{45}Sc. Green long-dashed line is the optical model; solid magenta line is an extrapolation based on the equation $L(E) = A_0 + B_0/E^{1.5}$; black dashed-dotted line is the standard CC calculation using a Woods-Saxon potential.

parameters ($V = 50$ MeV, $W = 10$ MeV, $r_0 = r_{0i} = 1.28$ fm, and $a_0 = a_{0i} = 0.4$ fm) were used. This set of parameters, suggested in Refs. [17,18], was used for many systems in our previous studies [11,19]. Larger uncertainties are assigned to these four data points.

The conversion of the fusion cross sections to either logarithmic derivatives, $L(E) = d\ln(\sigma E)/dE$ or S factors, $S(E) = \sigma E \exp(2\pi\eta)$ are given in Fig. 3. The stars for the $L(E)$ values were derived from the data by least-squares fits to three consecutive data points, while the solid circles were obtained with the two-points method. The dashed curve in Fig. 3(a) corresponds to the constant S-factor function $L_{cs}(E) = \frac{\pi\eta}{E}$, where η is the Sommerfeld parameter [5]. The solid (magenta) curve in Fig. 3(a) corresponds to a fit to the low-energy part of the experimental data with the formula proposed in Ref. [7]

$$L(E) = A_0 + B_0/E^{1.5} \ \text{MeV}^{-1}. \quad (1)$$

The solid (magenta) curves in Figs. 2 and 3(b) are, in turn, the extrapolated cross sections and S factors corresponding to the solid (magenta) curve in Fig. 3(a) with the equation

$$\sigma(E) = \sigma_s \frac{E_s}{E} e^{\{A_0(E-E_s) - B_0 \frac{1}{E_s^{1.5-1}(1.5-1)}[(\frac{E_s}{E})^{1.5-1}-1]\}}, \quad (2)$$

developed in Ref. [7]. Here σ_s is the fusion cross section at the energy E_s, which is the crossing point of the two functions $L(E)$ and $L_{cs}(E)$ and determines the energy location (E_s) of the S-factor maximum. The parameters E_s, L_s, A_0, B_0, and σ_s obtained from these two fits are summarized in Table I, together with the predictions obtained from the systematics of fusion hindrance developed in Ref. [19]. The predicted

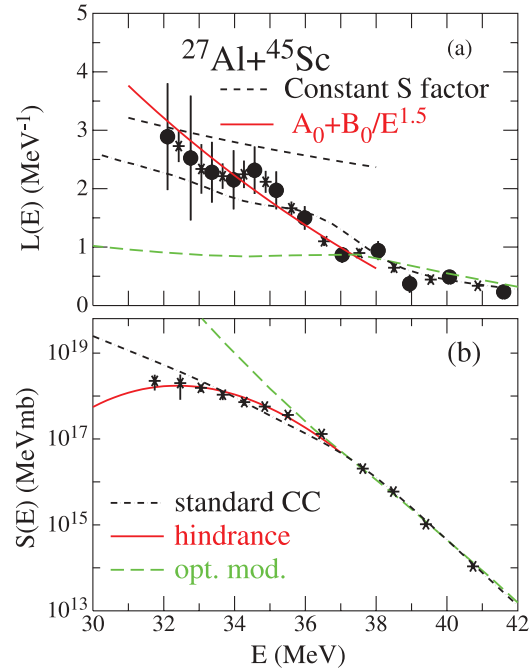

FIG. 3. (Color online) (a) The logarithmic derivative $L(E) = d(\ln \sigma E)/dE$ plotted as a function of the center-of-mass energy E. The stars were derived from the data by least-squares fits to three consecutive data points while the solid circles were obtained with the two-points method. The black dashed line is the constant S-factor function $L_{cs}(E)$. The solid magenta curve is a fit to the low-energy part of the data with a formula $L(E) = A_0 + B_0/E^{1.5}$. (b) The S factor versus E plot. The solid magenta curve is an extrapolated one (see text for details). The green long-dashed and the black dash-dotted curves are calculations from optical model and standard CC, respectively.

parameters agree well with the experimental values for the reaction ^{27}Al + ^{45}Sc.

III. COMPARISON WITH THEORETICAL CALCULATIONS

In many astrophysical applications fusion cross sections are needed at energies where no experimental data are available. The extrapolation into this energy region is usually done using the optical model. In these calculations it has to be taken into account, however, that the cross sections calculated in the optical model are the total reaction cross section, (i.e., the sum of fusion, inelastic, and transfer cross sections). It is well known [20] that, for heavier systems, inelastic excitations

TABLE I. Comparison of parameters obtained from the fusion reaction ^{27}Al + ^{45}Sc and from the systematics developed in Ref. [19]. L_s is the logarithmic derivative $L(E)$ at the energy E_s.

System	Method	E_s MeV	L_s MeV^{-1}	A_0 MeV^{-1}	B_0 MeV$^{1/2}$	σ_s μb
^{27}Al + ^{45}Sc	Exp.	32.4	3.01	−8.13	2052	1.6
	systematics	33.6	2.85	−9.32	2372	

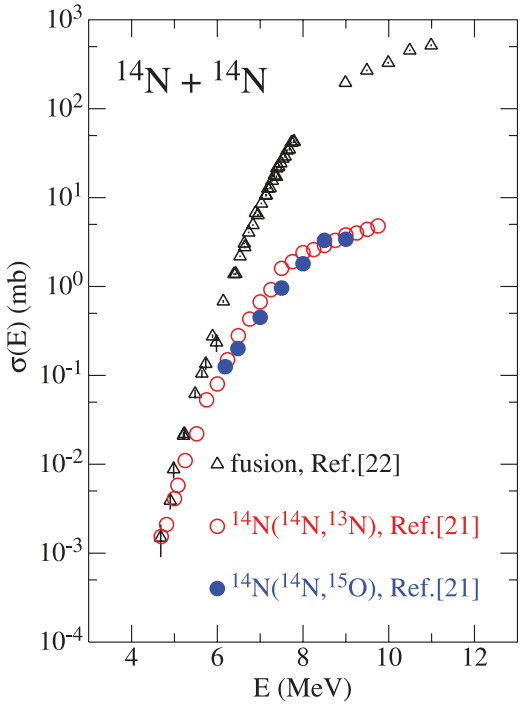

FIG. 4. (Color online) Comparison between experimental $\sigma(E)$ data for system ^{14}N + ^{14}N. Black triangles are for the fusion channel red-open and blue-solid circles are for neutron and proton transfer channels, respectively.

and transfer reactions can be orders of magnitude larger at lower energies than fusion cross sections. There are not many measurements of transfer cross sections at low energies published in the literature, especially for systems in the mass range $A = 12$–16. An example for the system ^{14}N + ^{14}N is shown in Fig. 4 for excitation functions of the one-neutron and one-proton transfer reactions (^{14}N,^{13}N) and (^{14}N,^{15}O) [21] together with the fusion cross sections [22]. With decreasing energy, the relative contributions of transfer reactions increase strongly and at the lowest energy the sum of the cross sections of the one-neutron and one-proton transfer reactions (^{14}N,^{13}N) and (^{14}N,^{15}O) are already higher than the fusion cross section itself. Due to the high excitation energy of the first excited state in ^{14}N ($E_x = 7.55$ MeV), the cross section for inelastic scattering is very low. In other systems, however, inelastic scattering may become the dominant reaction cross section and for that reason CC calculations (or other calculations of fusion cross sections) should be used to discuss the question of fusion enhancement or fusion hindrance.

For the system ^{27}Al + ^{45}Sc, optical model calculations with universal potential parameters [(green) long-dashed curves in Figs. 2 and 3] reproduce the excitation function down to about $E = 36$ MeV. At lower energies, the fusion cross section exhibits a much steeper fall-off and deviates from the optical model prediction by orders of magnitude. To study how much of this deviation is caused by the contributions from inelastic scattering and transfer reactions, CC calculations were performed. These include couplings to the ^{27}Al$_{g.s.}$($5/2^+$) ground state and to the excited $7/2^+$ and $9/2^+$ levels, which are considered to be members of a rotational band

TABLE II. Low-lying states in ^{27}Al included in the CC calculations (see Ref. [23]).

Isotope	J^π	E_x (MeV)	B ($E2$) (W.u.)
^{27}Al($5/2^+$)	$7/2^+$	2.21	14.0
	$9/2^+$	3.00	6.9

built on the ground state. The associated form factors for excitations of the ground-state rotational band are generated using a deformation parameter $\beta_2 = 0.345$, which is consistent with the quadrupole moment $Q_2 = 15$ fm^2, or the intrinsic quadrupole moment $Q_0 = 42$ fm^2. The parameters used in the calculations are listed in Table II (see Ref. [23]). Since the matrix elements for the excitation of ^{45}Sc are much weaker they were not included in the CC calculations. No data for transfer reactions in the system ^{27}Al + ^{45}Sc was found in the literature. Based on the behavior of other transfer reactions in this mass region [20,24], proton-stripping (^{27}Al,^{26}Mg) and proton-pickup reactions (^{27}Al,^{28}Si), which both have positive Q values, are included. The results of the CC calculations using a standard Woods-Saxon potential ($a = 0.63$ fm) are shown in Figs. 2 and 3 by black dash-dotted lines.

The CC calculations give a good description of the fusion cross section down to about 34 MeV. At even lower energies, however, they overpredict the fusion cross sections by factors of 3 or more.

In Ref. [25], an explanation of fusion hindrance was proposed that was based on the saturation property of nuclear matter. This model reproduced the hindrance behavior observed in many systems with negative Q values, for example, ^{64}Ni + ^{64}Ni [25], ^{64}Ni + ^{100}Ni [26], ^{28}Si + ^{64}Ni [1], and ^{16}O + ^{208}Pb [27]. Recently, the same recipe with similar parameters was used to describe the hindrance behavior for fusion reactions with positive Q values (e.g. ^{28}Si + ^{30}Si [11] and ^{16}O + ^{16}O [28]).

The same model was then adopted in the calculations of the fusion cross sections for the system ^{27}Al + ^{45}Sc. The potential used in the model is a M3Y potential with the addition of a repulsive core [25], which is based on a nuclear incompressibility of $K = 234$ MeV and a diffuseness a_{rep} of the hard core density, varying within the 0.40–0.44 fm range. Potentials calculated with these parameters are compared in Fig. 5 to the pure M3Y and the standard Woods-Saxon potentials [29]. It should be mentioned that the potentials are slightly different for the different substates $m = 1/2$, $3/2$, and $5/2$ while average values are used in Fig. 5. It is evident that the introduction of a repulsive potential leads to a shallower pocket and a larger barrier width and thus to a reduction in the fusion cross section.

A comparison of the S factors calculated from various potentials with the experimental data is presented in Fig. 6. The black dash-dotted curve is the result of standard CC calculations (with a Woods-Saxon potential), which overpredict the cross sections at several of the lowest energy points. Calculations using the shallow potential model reproduce the experimental data much better. The best agreement with the present data is achieved with $a_{rep} = 0.40$ fm as shown by

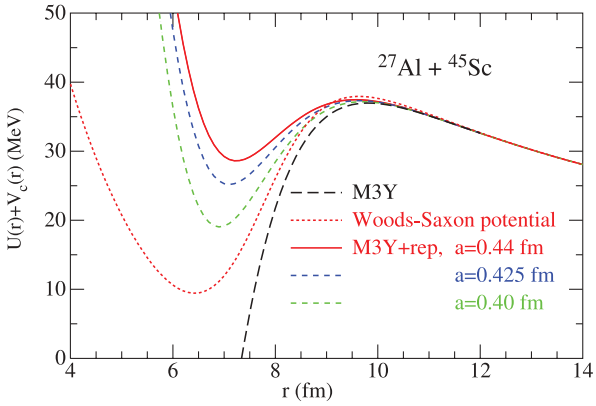

FIG. 5. (Color online) Comparison of potentials used in the CC calculations. Different stiffnesses $a_{\rm rep}$ of the hard core density are used ($a_{\rm rep} = 0.40$, 0.425, and 0.44 fm, respectively), see Ref. [25]. The black long-dashed curve is the pure M3Y potential and the red dotted curve is the Woods-Saxon potential from Ref. [29].

the (light-blue) dotted curve. With an even shallower potential (e.g., with $a_{\rm rep} = 0.44$ fm) an S-factor maximum appears in the calculations [(blue) dashed line], which is similar to the (red) curve obtained from an extrapolation based on the fusion hindrance recipe [7] (the same curve is shown in Figs. 2 and 3). For systems studied previously, most of them are fusion reactions between two even-even nuclei, the best value of $a_{\rm rep}$ used was 0.415 fm.

As can be seen from Fig. 3, the experimental values of the logarithmic derivative $L(E)$ just reached the constant S-factor value. As a result, the $S(E)$ curve has leveled off, but no maximum in the S factor can be observed. While it is not necessary for systems with positive Q values to have an S-factor maximum, it will, however, be very interesting to extend measurements for some of the systems to lower energies

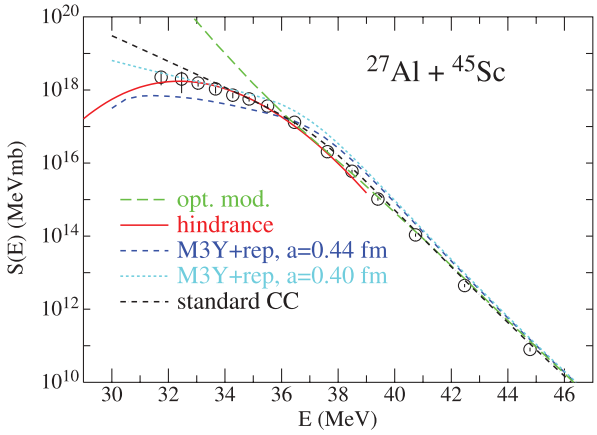

FIG. 6. (Color online) Comparison between the experimental $S(E)$ curve for the fusion reaction ^{27}Al + ^{45}Sc and various calculations. The black dash-dotted and green long-dashed curves are calculations from standard CC (with a Woods-Saxon potential) and optical model. The blue dashed and light-blue dotted curves are CC calculations from a shallow potential and with $a_{\rm rep} = 0.44$ and 0.40 fm, respectively. The red solid line is the extrapolation with the hindrance recipe.

to examine whether an S-factor maximum does develop in these systems. For this purpose, the lower cross-section limit in the experiment has to be pushed down by another order of magnitude.

IV. RESULTS FROM OTHER SYSTEMS WITH POSITIVE Q VALUES

Three excitation functions for fusion reactions with positive (^{28}Si + ^{30}Si [11] and ^{27}Al + ^{45}Sc) or slightly negative (^{28}Si + ^{64}Ni [1]) Q value, measured recently at ATLAS are compared in Fig. 7. The lowest cross sections ($\sigma_{\rm min}$) measured in these experiments are listed in Figs. 7(b), 7(d), and 7(f), respectively. The behavior of these three systems for both $L(E)$ and $S(E)$ is very similar. At the lowest energies, standard CC calculations [shown by the (blue) dashed-dotted curves] overpredict the cross sections. An S-factor maximum is observed only for the system ^{28}Si + ^{64}Ni where the Q value is slightly negative, but where the cross sections can be measured down to 26 nb. For the other two systems, ^{28}Si + ^{30}Si and ^{27}Al + ^{45}Sc, the measurements need to be extended to lower energies before a similar conclusion can be reached.

The solid (magenta) curves are fits of low-energy data to Eq. (1) [in (a), (c), and (e)[1]] and are corresponding extrapolations [Eq. (2)] in the S-factor representations (b), (d), and (f), respectively.

A similar series of measurements was recently performed at Legnaro. In Fig. 8, results for the system ^{36}S + ^{48}Ca [12] ($Q = 7.55$ MeV) are compared with measurements in two other systems ^{48}Ca + ^{48}Ca and ^{40}Ca + ^{40}Ca [13,30,31]. The lowest cross sections ($\sigma_{\rm min}$) measured in these experiments are also listed in the figures. The (red) arrows in Fig. 8 (and also in Fig. 7) give the predicted energy locations of the S-factor maximum, obtained from the hindrance systematics (see Ref. [19], which surveyed the fusion excitation functions of "stiff" systems from medium-mass nuclei down to lighter systems around ^{16}O + ^{16}O)

$$L_s^{\rm emp} = 2.33 + 580/\zeta \ \ ({\rm MeV}^{-1}), \tag{3}$$

and

$$E_s^{\rm emp} = [0.495\zeta / L_s^{\rm emp}(\zeta)]^{2/3} \ \ ({\rm MeV}). \tag{4}$$

The results of $S(E)$ and $L(E)$ for the systems ^{36}S + ^{48}Ca and ^{48}Ca + ^{48}Ca are very similar, though there is a big difference between their fusion Q values: 7.55 and -2.99 MeV, respectively. An exponential increase of $S(E)$ with decreasing energy is followed by a change in slope at the lowest energies, where the slope falls below the standard CC predictions [(blue) dash-dotted curves]. That is, hindrance behaviors are observed in these systems as well as for those shown in Fig. 7. It seems, however, that the detailed patterns of these $S(E)$ and $L(E)$ curves are different from those observed in Fig. 7. For these two systems, no S-factor maximum was

[1]Because the Q value is negative for the system ^{28}Si + ^{64}Ni, the factor $E^{1.5}$ in Eq. (1) should be replaced by $(E + Q)^{1.5}$

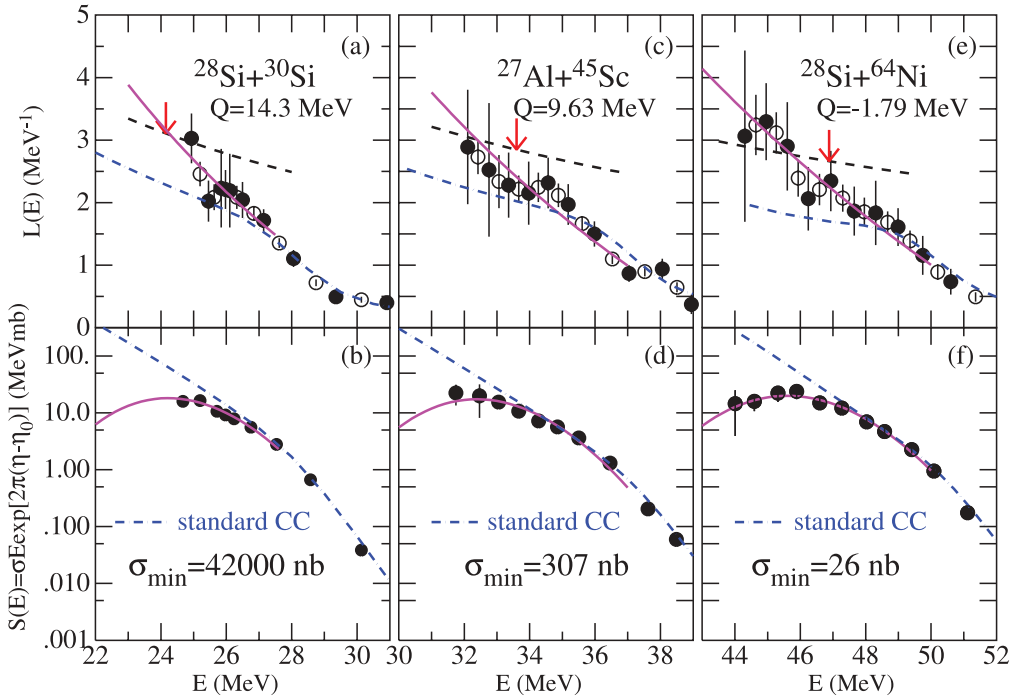

FIG. 7. (Color online) $L(E)$ [(a), (c), and (e)] and $S(E)$ [(b), (d), and (f)] plots for the reactions ^{28}Si + ^{30}Si, ^{27}Al + ^{64}Ni and ^{28}Si + ^{64}Ni. The black dashed curves display the constant S-factor functions and the red arrows are energy locations of S-factor maxima predicted by the hindrance systematics [from Eqs. (3) and (4)]. The blue dash-dotted curves are from standard CC calculations with a standard Woods-Saxon potential and the magenta curves represent fits to $L(E)$ data at the low-energy region [(a), (c), and (e), with Eq. (1)] and to the extrapolations in the S-factor representation [(b), (d), and (f)]. In (a), (c), and (e), solid and open circles correspond to slope determinations from consecutive data points and least-squares fits to three data points, respectively. The lowest cross sections (σ_{min}) measured in these experiments are included in (b), (d), and (f), respectively.

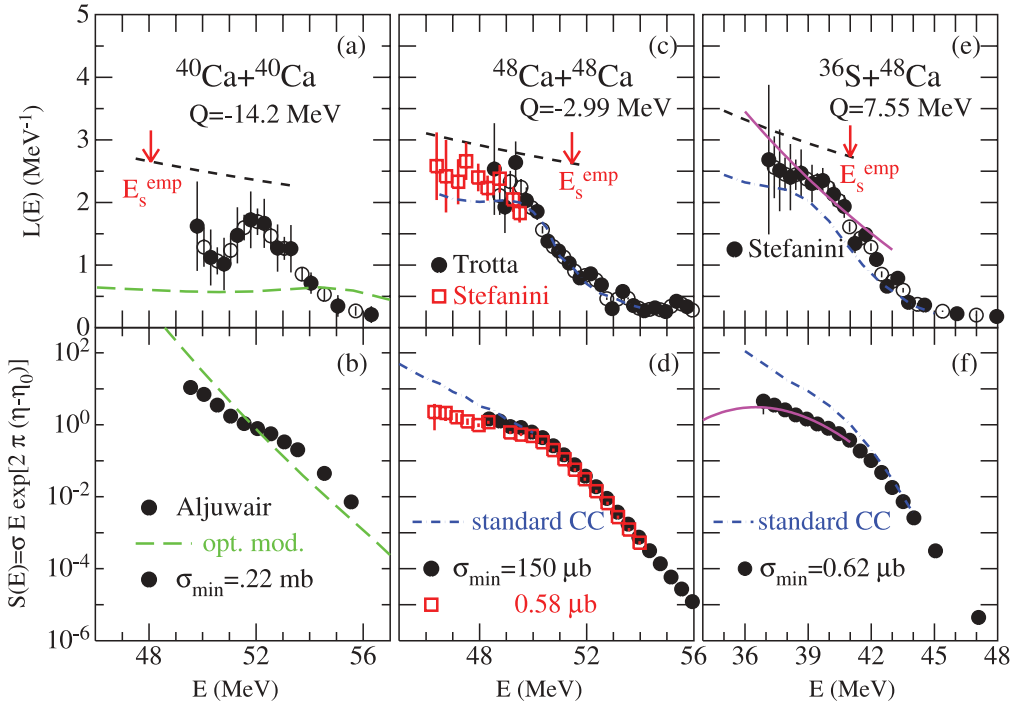

FIG. 8. (Color online) $L(E)$ [(a), (c), and (e)] and $S(E)$ [(b), (d), and (f)] plots for the reactions ^{40}Ca + ^{48}Ca, ^{48}Ca + ^{48}Ca, and ^{36}S + ^{48}Ca. The black dashed curves, the red arrows, the blue dash-dotted curves, and the magenta curves have the same meanings as in Fig. 7. The lowest cross sections (σ_{min}) measured in these experiments are included in (b), (d), and (f), respectively.

observed in the measured energy regions (already much lower than the predicted values of $E_s^{\rm emp}$). Nevertheless, since the Q value of ^{48}Ca + ^{48}Ca is negative, there should be an S-factor maximum. It should be mentioned that the energy values of $E_s^{\rm emp}$ have to be considered as upper limits since most of the systems in Figs. 7 and 8 do not involve "stiff" nuclei. One possibility can be that the higher neutron excess N-Z for the systems ^{48}Ca + ^{48}Ca and ^{36}S + ^{48}Ca push the fusion hindrance to lower energies (a similar situation happens for medium-mass systems [1]). However, for system ^{40}Ca + ^{40}Ca [Figs. 8 and 8(b)], the neutron excess N-Z is low, correspondingly $E_s^{\rm emp}$ is located lower than the measured energy region and behaviors of $S(E)$ and $L(E)$ for system ^{40}Ca + ^{40}Ca are rather similar to those shown in Fig. 7. Clearly, an extension of these measurements into the 20 nb region is urgently needed.

V. CONCLUDING REMARKS

An attempt to measure heavy-ion fusion hindrance in a lighter system with a positive Q value ^{27}Al + ^{45}Sc is reported. While the excitation function was measured to cross sections as low as 300 nb, it was still not sufficient to observe a clear maximum in the S-factor representation.

The experimental data are compared to various theoretical predictions. The optical model calculates the total reaction cross sections that include contributions from reactions other than fusion. Thus, contributions from transfer reactions and inelastic excitations, which may be relatively strong at low energies, have to be subtracted. These contributions from other reaction channels were not considered in the extrapolations performed previously and this is one of the reasons that those predictions are considerably higher than the experimental data. For this reason, CC or other codes explicitly calculating fusion cross sections should be used in the extrapolations.

A comparison of the data with CC calculations indicates that experimental cross sections are smaller than the standard CC predictions, confirming the occurrence of fusion hindrance in a system with positive Q value. So far, none of the systems with positive Q values has shown a maximum in the S-factor representation. Therefore, fusion measurements that were performed down to the ∼300 nb region for systems with positive Q values need to be improved further by at least another order of magnitude. This is a considerable challenge due to the contributions from background reactions originating, at least in part, from ubiquitous target contaminants.

ACKNOWLEDGMENTS

The authors thank A.M. Stefanini and G. Montagnoli for valuable discussions. This work was supported by the US Department of Energy, Office of Nuclear Physics, under Contract No. DE-AC02-06CH11357.

[1] C. L. Jiang *et al.*, Phys. Rev. Lett. **89**, 052701 (2002); **93**, 012701 (2004); Phys. Rev. C **71**, 044613 (2005); Phys. Lett. **B640**, 18 (2006).
[2] M. Dasgupta, D. J. Hinde, A. Diaz-Torres, B. Bouriquet, C. I. Low, G. J. Milburn, and J. C. Newton, Phys. Rev. Lett. **99**, 192701 (2007).
[3] M. Trotta *et al.*, Nucl. Phys. **A787**, 134c (2007).
[4] G. Montagnoli, in AIP Conference Proceedings of Fusion08, Chicago, 22–26 Sept. 2008.
[5] C. L. Jiang, H. Esbensen, B. B. Back, R. V. F. Janssens, and K. E. Rehm, Phys. Rev. C **69**, 014604 (2004).
[6] C. L. Jiang, B. B. Back, H. Esbensen, R. V. F. Janssens, and K. E. Rehm, Phys. Rev. C **73**, 014613 (2006).
[7] C. L. Jiang, K. E. Rehm, B. B. Back, and R. V. F. Janssens, Phys. Rev. C **75**, 015803 (2007).
[8] C. L. Jiang, B. B. Back, R. V. F. Janssens, and K. E. Rehm, Phys. Rev. C **75**, 057604 (2007).
[9] L. R. Gasques *et al.*, Phys. Rev. C **76**, 035802 (2007).
[10] M. Wiescher, in AIP Conference Proceedings of Fusion08, Chicago, 22–26 Sept. 2008; D. Yakovlev, Bulletin of the American Physical Society, April Meeting of 2008, St. Louis, Missouri, p. 128 (J14-1); http://www.er.doe.gov/.np/nsac/does/Nuclear-Science.High-Res.pdf (2007).
[11] C. L. Jiang *et al.*, Phys. Rev. C **78**, 017601 (2008).
[12] A. Stefanini *et al.*, Phys. Rev. C **78**, 044607 (2008).
[13] A. Stefanini *et al.*, Phys. Lett. **B679**, 95 (2009).
[14] C. N. Davids and J. D. Larson, Nucl. Instrum. Methods Phys. Res. B **40-41**, 1224 (1989); C. N. Davids *et al.*, *ibid.* **70**, 358 (1992).
[15] C. L. Jiang *et al.*, Nucl. Instrum. Methods A **554**, 500 (2005).
[16] A. Gavron, Phys. Rev. C **21**, 230 (1980).
[17] G. J. Michaud and E. W. Vogt, Phys. Rev. C **5**, 350 (1972); G. J. Michaud, *ibid.* **8**, 525 (1973).
[18] R. G. Stokstad *et al.*, Phys. Rev. Lett. **37**, 888 (1976).
[19] C. L. Jiang, K. E. Rehm, B. B. Back, and R. V. F. Janssens, Phys. Rev. C **79**, 044601 (2009).
[20] K. E. Rehm, Annu. Rev. Nucl. Part. Sci. **41**, 429 (1991).
[21] R. M. Gaedke *et al.*, Phys. Rev. **141**, 996 (1966).
[22] Z. E. Switkowski *et al.*, Nucl. Phys. **A274**, 202 (1976).
[23] H. Esbensen, Phys. Rev. C **68**, 034604 (2003).
[24] M. F. Vineyard *et al.*, Phys. Rev. C **33**, 1325 (1986).
[25] Ş. Mişicu and H. Esbensen, Phys. Rev. Lett. **96**, 112701 (2006).
[26] Ş. Mişicu and H. Esbensen, Phys. Rev. C **75**, 034606 (2007).
[27] H. Esbensen and Ş. Mişicu, Phys. Rev. C **76**, 054609 (2007).
[28] H. Esbensen, Phys. Rev. C **77**, 054608 (2008).
[29] Ö. Akyüz and A. Winther, in *Proceedings of the Enrico Fermi School of Physics, 1979, Course on Nuclear Structure and Heavy Ion Reactions*, edited by R. A. Broglia, C. H. Dasso, and R. Ricci (North Holland, Amsterdam, 1981).
[30] M. Trotta, A. M. Stefanini, L. Corradi, A. Gadea, F. Scarlassara, S. Beghini, and G. Montagnoli, Phys. Rev. C **65**, 011601(R) (2001).
[31] H. A. Aljuwair *et al.*, Phys. Rev. C **30**, 1223(R) (1984).